Arch. Metall. Mater. **65** (2020), 1, 151-156

DOI: 10.24425/amm.2019.131108

H. KRAWIEC[1*], V. VIGNAL[2], J. LELITO[1], A. KRYSTIANIAK[2], E. TYRAŁA[1]

INFLUENCE OF THE HEAT TREATMENT ON THE MICROSTRUCTURE AND CORROSION RESISTANCE OF AUSTEMPERED DUCTILE IRON (ADI)

The influence of the hold time of the austempering heat treatment at 280°C on the microstructure and corrosion resistance in NaCl-based media of austempered ductile iron was investigated using X-ray diffraction, micro-hardness measurements, corrosion tests and surface observations. Martensite was only found in the sample which was heat treated for a short period (10 minutes). Corrosion tests revealed that this phase does not play any role in the anodic processes. Numerous small pits were observed in the α-phase which is the precursor sites in all samples (whatever the value of the hold time of the austempering heat treatment).

Keywords: austempered ductile iron, corrosion, microstructure, heat treatment

1. Introduction

Austempered ductile iron (ADI) is widely used in numerous industries (such as automotive, agriculture and energy) because of its high strength and ductility, good wear resistance and high fatigue strength compared to ductile iron (DI) [1-4]. These good mechanical properties result from a specific microstructure which is composed of graphite spheres in an "ausferrite" matrix (mixture of ferrite, α-phase, and high carbon austenite, γ_{HC}-phase). ADI is obtained by applying an austempering heat treatment to DI. This heat treatment is divided into three steps: (i) DI is heated at a temperature of about 900°C (formation of an austenitic matrix, γ-phase), (ii) the metal is cooled down to a temperature in the range of 250-450°C (austempering temperature) and held at that temperature for the required time and (iii) the casting is water cooled to room temperature. During the step (ii), γ-phase decomposes into α-phase and γ_{HC}-phase. If the casting is held at the austempering temperature for a too short period (ie before the incubation time of ferrite nucleation), γ-phase which is not yet decomposed transforms into martensite during water cooling. On the other hand, if the casting is held at the austempering temperature for a too long period, γ_{HC}-phase decomposes into α-phase and ε-carbides (bainite). The presence of martensite or bainite in ADI has detrimental influence on the mechanical properties [1-4] of ADI. The corrosion behaviour of ADI has already been studied in sulphuric acid [5], sodium perchlorate at pH = 3 [6] and pH = 10 [7]. The influence of the austempering temperature on the microstructure and pitting corrosion of ADI in NaCl-based solutions has also been investigated [8]. The obtained results show that the microstructure plays a key role in the corrosion behaviour of ADI.

In the present paper, the influence of the hold time of the austempering heat treatment at 280°C (for 10 or 150 minutes) on the microstructure and corrosion resistance in NaCl-based media of ADI is investigated.

2. Materials and methods

2.1. Materials and surface preparation

The chemical composition of DI used is C: 3.48 wt.%, Mn: 0.63%, Si: 2.58%, P: 0.03%, S: 0.017%, Cr: 0.06%, Ni: 0.04%, Cu: 0.32%, Mg: 0.054%, Mo: 0.07%, Ti: 0.015%, Sn: 0.006%, Pb: 0.001%, V: 0.009%, W: 0.038%, Zn: 0.003. This heat treatment procedure was applied: (1) austenitizing at 900°C for 2 hours, (2) austempering at 280°C for 10 minutes (sample 1.1) and for 150 minutes (sample 7.1), (3) water cooling down to room temperature. The heat treatment was performed in a salt bath furnace. Before corrosion tests, ADI samples were embedded in

[1] AGH UNIVERSITY OF SCIENCE AND TECHNOLOGY, FACULTY OF FOUNDRY ENGINEERING, 23 REYMONTA STR., 30-059 KRAKÓW, POLAND
[2] ICB UMR 6303 CNRS – UNIVERSITÉ BOURGOGNE FRANCHE-COMTÉ, DIJON, FRANCE

* Corresponding author: krawiec@agh.edu.pl

an epoxy resin, mechanically ground with silicon carbide (SiC) emery papers down to 4000 grit, polished with diamond pastes down to 1 μm and ultrasonically rinsed in ethanol.

2.2. Corrosion tests

Electrochemical corrosion tests were performed in 0.05 M NaCl (aerated solution) at 25°C using a classical three-electrode cell and a PGSTAT302N AUTOLAB potentiostat/galvanostat. All potentials were measured vs. saturated calomel (SCE) reference electrode. The counter electrode was made of platinum disk (diameter of 1 cm). Polarisation curves were plotted at a potential scan rate of 1 mV/s, from an applied potential of –0.5 V vs. SCE (cathodic domain). No prior polarisation in the cathodic domain was applied to the system. The corrosion behaviour of samples was also studied using the potentiostatic pulse technique (PPT) method. It consists in applying a potential E_A (0.1 V vs the OCP value) for 1 second and then a potential of –0.7 V vs. SCE in the cathodic domain (passive behaviour) for 1 second. This procedure was repeated 3 cycles.

2.3. Surface observations and physical-mechanical analysis

After corrosion tests, the specimen surface was cleaned in ethanol under ultrasonics and then observed by FE-SEM coupled with an EDS (JEOL 7600F). This equipment was used to identify active sites and to determine the chemical composition of phases and corrosion products at the micro-scale.

XRD analysis was performed after mechanical polishing using CuKα (λ = 1.54 Å) as radiation source. Measurements were carried out with a Bruker D8-A25-Advance diffractometer and a LynxEye detector. XRD diffractograms were fitted using the Topas software package and the Rietveld method (structural model) [9].

Microhardness tests were carried out after etching with nital (to reveal the microstructure) with an applied load of 25 gf (gram-force) using low-load Vickers micro-indentation hardness testing (Micromet 5114 with Omninet image acquisition and analysis software from Buehler). This load was applied for 10 seconds. The microhardness values are an average of four measurements (the error is the standard deviation).

3. Results and discussion

3.1. Microstructure of samples

The microstructure of the two samples was first revealed by etching with nital, as shown in Fig. 1(a-d) and 2(a-d). For both samples, the "ausferrite" matrix was revealed. It consists of a plates (generally oriented perpendicularly to the surface) and g_{HC} between them. The microstructure of the two samples was very fine (Fig. 1(d) and 2(d)) and it was not possible to determine

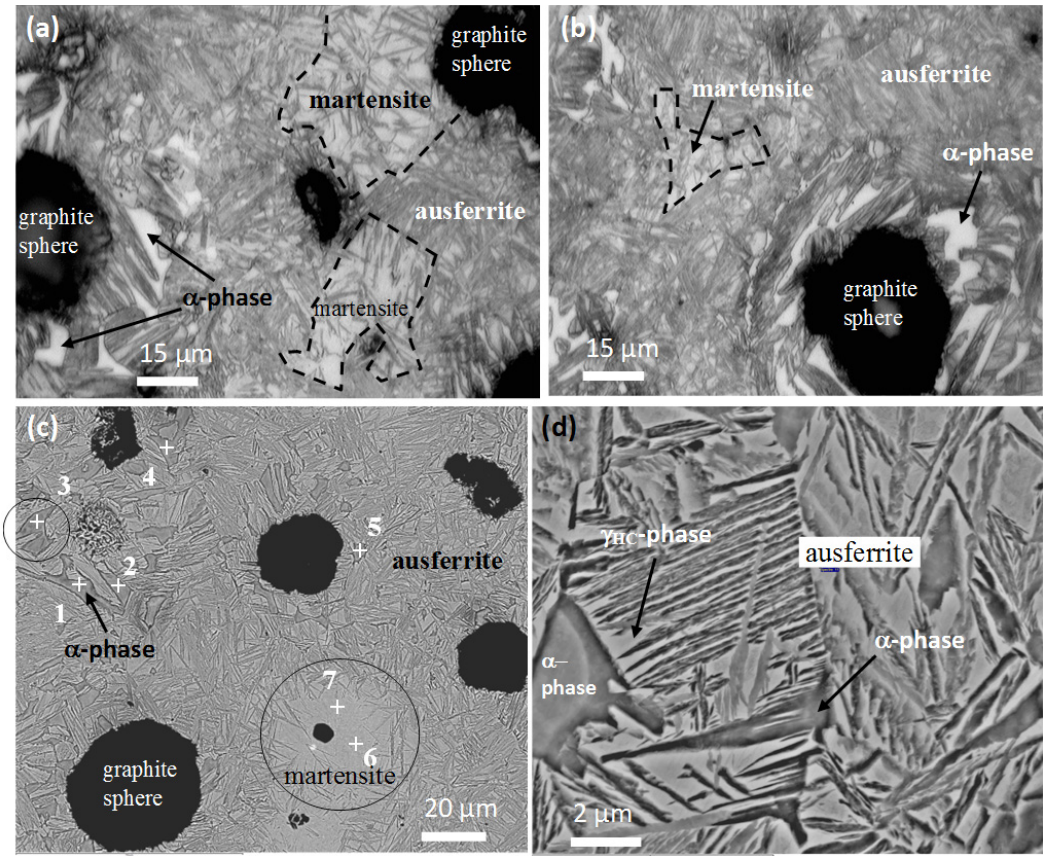

Fig. 1. (a-b) Optical and (c-d) FE-SEM images of sample 1.1 etching with nital for 10 seconds

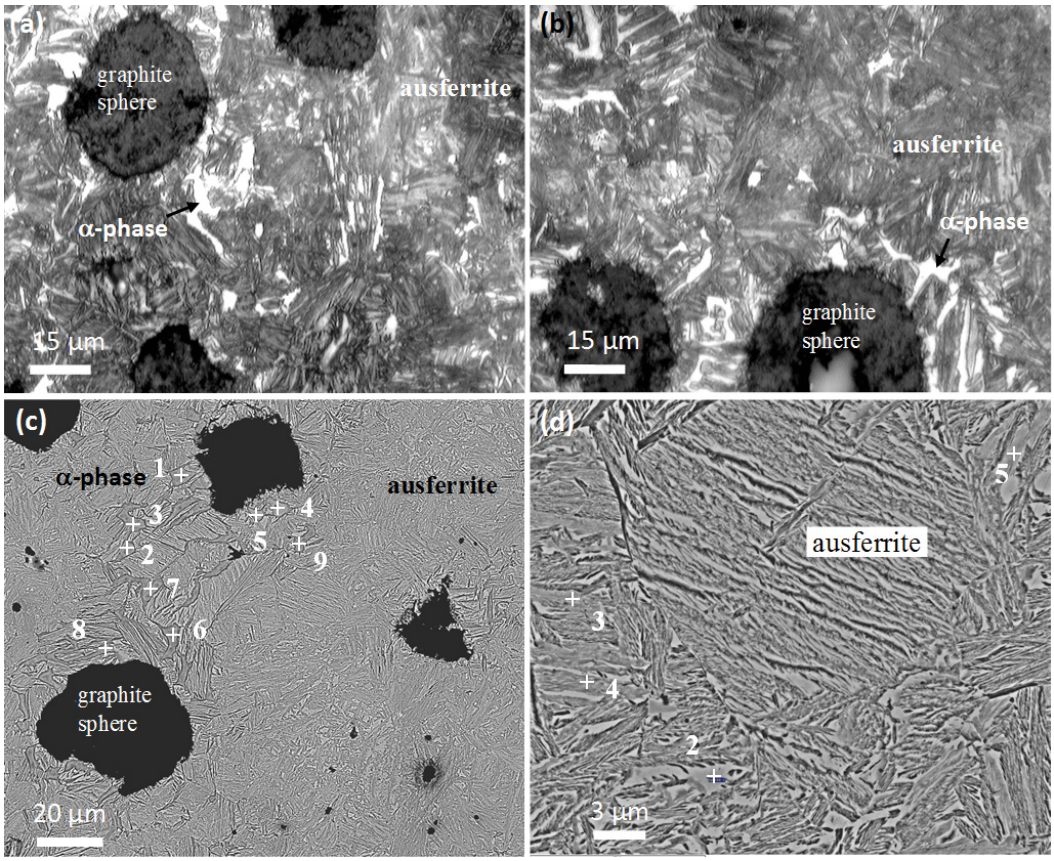

Fig. 2. (a) optical and (b) FE-SEM images of sample 7.1 etching with nital for 10 seconds

the composition of each phase using FE-SEM/EDS. However, analyses in sites containing the two phases give:

Sample 1.1: 11.4 ± 1.1% C*, 3.3 ± 0.6% O*, 4.3 ± 0.2% Si, 0.5 ± 0.1% Mn, 80.5 ± 1.4% Fe

Sample 7.1: 10.6 ± 0.9% C*, 2.5 ± 0.7% O*, 3.9 ± 0.2% Si, 0.7 ± 0.1% Mn, 82.2 ± 1.1% Fe

Therefore, the two "ausferrite" matrices (samples 1.1 and 7.1) have the same composition. They contain a large amount of Si (from α-phase) and carbon (from γ_{HC}-phase). It is always difficult to estimate the amount of carbon in samples by means of FE-SEM/EDS. The micro-hardness was evaluated in the two 'ausferrite' matrices at 596.5 ± 7.9 HV_{25}.

Some ferrite (α-phase) plates oriented parallel to the specimen surface were also revealed in the two samples (sites 1-5 in Fig. 1(c) and sites 1-9 in Fig. 2(c)). EDS analyses in these sites give in average (at.%, error = standard deviation):

Sample 1.1: 6.7 ± 0.6% C*, 1.9 ± 0.6% O*, 6.9 ± 0.8% Si, 0.2 ± 0.1% Mn, 84.3 ± 0.8% Fe

Sample 7.1: 6.7 ± 0.9% C*, 2.3 ± 0.3% O*, 6.6 ± 0.9% Si, 0.3 ± 0.2% Mn, 84.2 ± 1.3% Fe

As expected, they contain a large amount of Si and a low amount of Mn and C. Regions depleted in ferrite (α-phase) plates were only found in sample 1.1 (sites 6-7 in Fig. 1(c)). Such regions were not observed in sample 7.1. FE-SEM/EDS analyses in these regions give in average (at.%, error = standard deviation): 11.2 ± 0.9% C*, 2.2 ± 0.1% O*, 3.4 ± 0.1% Si, 1.0 ± 0.1% Mn and 81.6 ± 0.9% Fe. Therefore, they are enriched in carbon and manganese. They correspond to martensite, resulting from the transformation of austenite during the water cooling. In sample 1.1, the austenite was not completely decomposed into α- and γ_{HC}-phases during the austempering heat treatment. Note that martensite was observed in numerous regions using optical microscopy and FE-SEM/EDS, Fig. 1(a-c). The micro-hardness was evaluated in this zone at 1022.3 ± 56.7 HV_{25}. This site is then significantly harder than the 'ausferrite' matrix, confirming that it is martensite. In sample 7.1, austenite was completely decomposed into α- and γ_{HC}-phases and no martensite was identified.

Fig. 3 shows the XRD diffractograms of the two samples after mechanical polishing. For both samples, two crystallographic

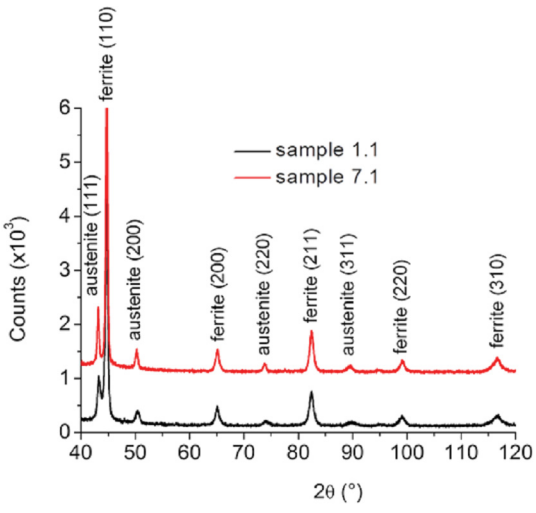

Fig. 3. XRD diffractogramms of the sample 1.1 and 7.1 after polishing

systems were identified, namely the face-centred cubic (fcc) and body-centred cubic (bcc) systems. XRD analyses indicate that the fcc / bcc ratio is very close in the two samples (20.3 / 79.7 for sample 1.1 and 19.2 / 80.8 for sample 7.1). For both samples, the fcc system corresponds to the γ_{HC}-phase. For sample 7.1, the bcc system corresponds only to the α-phase. By contrast, for sample 1.1, this system is attributed to both α-phase and martensite. It was not possible to distinguish the ferrite / martensite ratio from XRD analysis.

3.2. Corrosion behaviour in 0.05M NaCl (aerated solution) at 25°C

Fig. 4(a) shows the polarisation curves of samples 1.1 and 7.1 in 0.05M NaCl (aerated solution) at 25°C. The current plateau observed in the cathodic branch is related to the oxygen diffusion-limited reduction reaction. Indeed, under the selected conditions, the main reduction reaction is the oxygen reduction reaction (reaction 1).

$$O_2 + 2H_2O + 4e^- \rightarrow 4OH^-,\ E^0 = 0.156\ V\ vs\ SCE \qquad (1)$$

The cathodic domain is observed over a wider potential range on sample 1.1 than on sample 7.1. This leads to a shift of the potential corrosion between the two samples of about 100 mV. These differences may be explained by the presence of martensite in sample 1.1. The influence of martensite on the current density in the cathodic branch is still under study.

No passive range was found in the anodic domain, indicating that the two samples are active in this aqueous solution. Surface observations performed at low spatial resolution after polarisation curves show that graphite spheres are not dissolved.

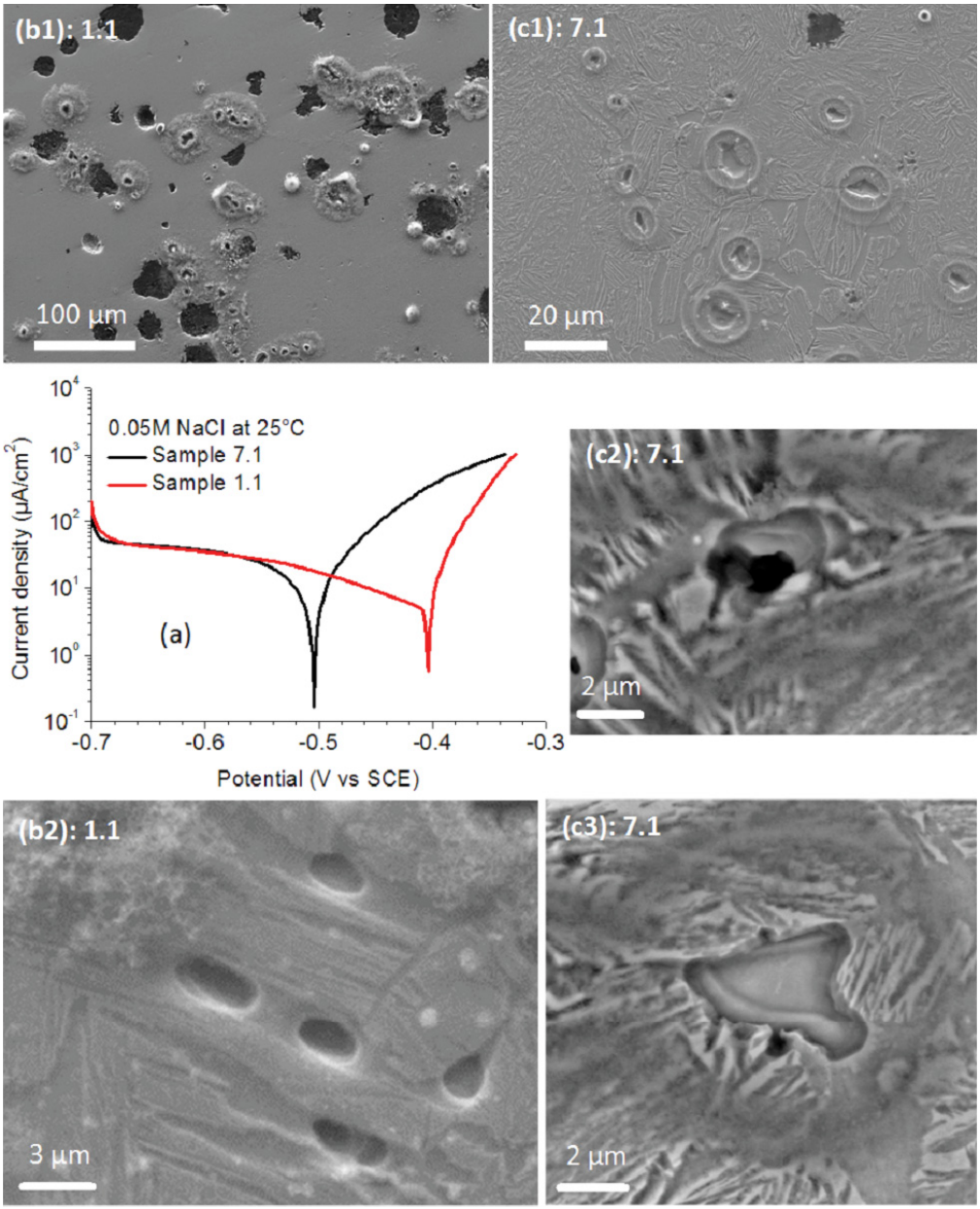

Fig. 4. Polarisation curves (1 mV/s) of samples 1.1 and 7.1 in 0.05 M NaCl at 25°C. (b-c) FE-SEM images of the two samples after the polarisation curve

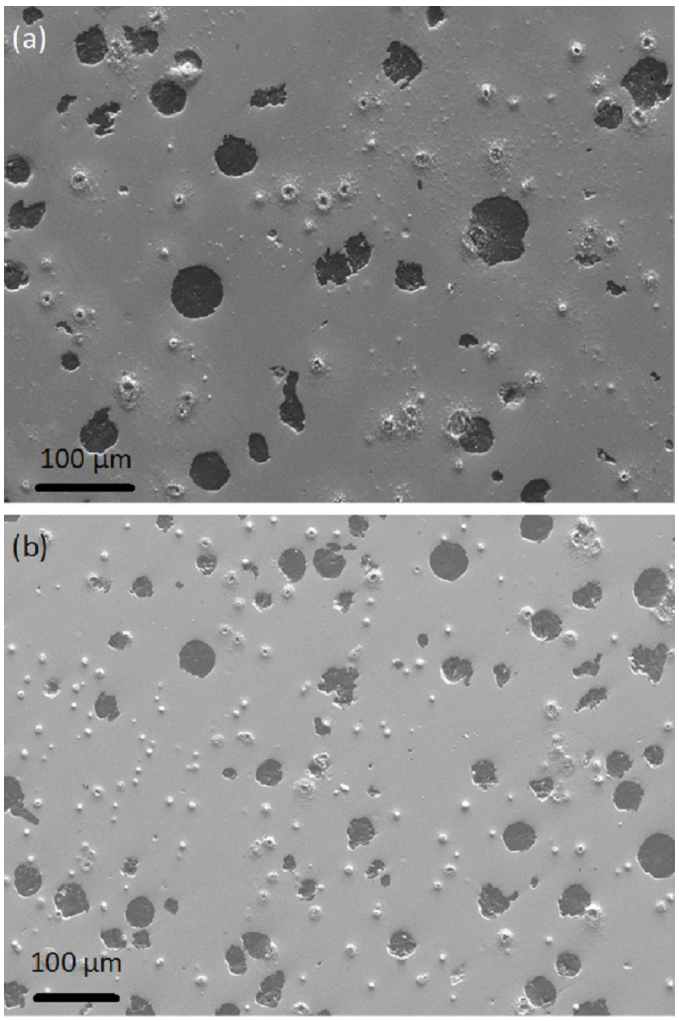

Fig. 5. FE-SEM/EDS images at low spatial resolution of (a) sample 1.1 and (b) sample 7.1 after PPT test

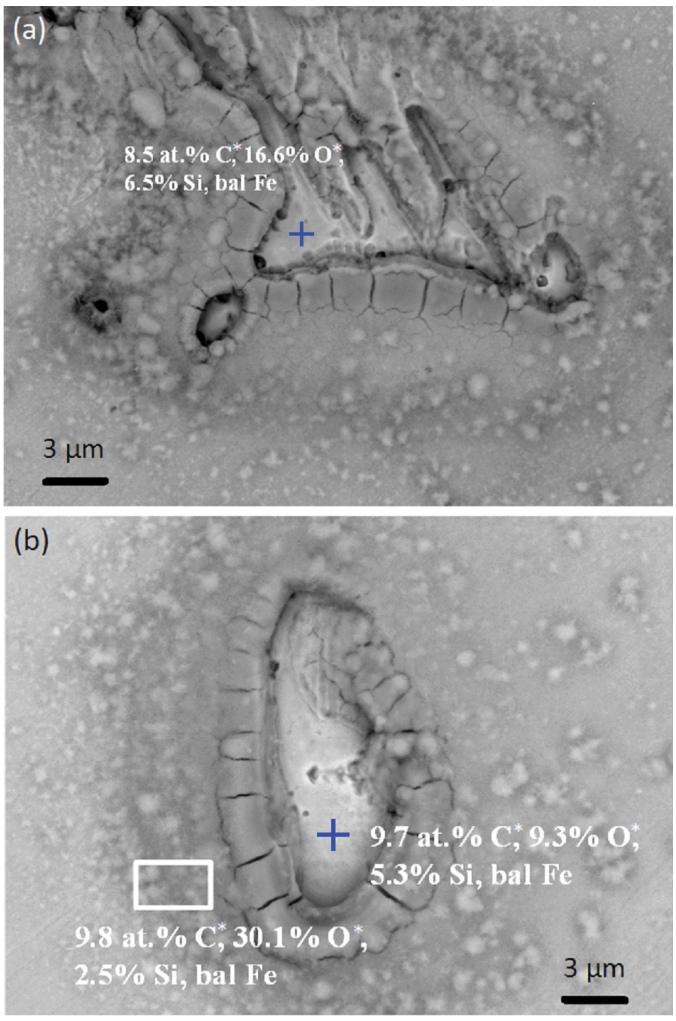

Fig. 6. (a-b) FE-SEM/EDS images at high spatial resolution of sample 1.1 after PPT test

A large number of pits initiate in the matrix (Fig. 4(b1) and 3(c1)). Only a few pits initiate at the graphite spheres / matrix interface. By contrast, numerous pits initiate at these interfaces in $NaClO_4$ solutions, pH = 10 [7]. Corrosion products are systematically observed in active sites. Surface observations at high spatial resolution show that the α-phase is preferentially dissolved in both samples, Fig. 4(b2), 4(c2) and 4(c3). Indeed, numerous small pits are visible in this phase. This demonstrates that the α-phase is the precursor site for pitting in ADI in 0.05M NaCl (aerated solution) at 25°C. Martensite which is only present in sample 1.1 does not play any role in the anodic processes.

To confirm the previous assumptions, PPT was performed on both samples. This test first confirms that a large majority of pits initiate in the matrix, Fig. 5(a)-(b). Only a few ones are found at the interface between graphite spheres and the matrix. Corrosion products are also systematically formed around active sites. Therefore, the way of applying potential (polarisation curves vs PPT) has no influence on the obtained results and on corrosion mechanisms. Surface observations at high spatial resolution after PPT reveal the existence of numerous very small pits in the α-phase, Fig. 6(a)-(b) and Fig. 7, which acts as anodic site. FE-SEM/EDS analyses (see numerical values in Fig. 6(a)-(b) and Fig. 7) indicate that there is no preferential dissolution of alloying elements in the α-phase. Indeed, roughly the same C, Si, and Fe contents were found than after polishing. Only the oxygen content is significantly increased due to oxidation.

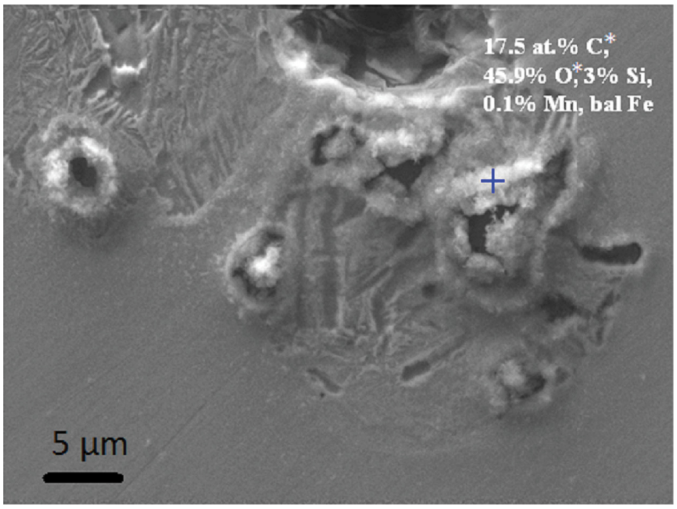

Fig. 7. FE-SEM/EDS image at high spatial resolution of sample 7.1 after PPT test

FE-SEM/EDS analyses confirm the presence of corrosion products around the α-phase. They are mainly composed of oxygen and iron (iron oxides / hydroxides).

4. Conclusions

A multi-disciplinary approach, based on microstructural investigations, mechanical measurements (micro-hardness) and corrosion tests, was applied to ADI samples after various austempering heat treatments (10 or 150 minutes at 280°C). Obtained results confirm that martensite is only detected in ADI after short hold time. However, this phase has no role in corrosion. Precursor sites are located in the ferrite. Numerous small pits were observed in this phase in 0.05 M NaCl (aerated solution) at 25°C. Therefore, improving the corrosion resistance of ADI necessitates improving the behaviour of the α-phase (by introducing compressive stresses or by slightly changing its composition, for example).

(*) Note: C and O were determined from the stoichiometry and results of micro-analysis of other elements, taking into account the specificity of the occurring corrosion phenomena.

REFERENCES

[1] B.V. Kovacs, AFS Trans. **102**, 417-420 (1994).

[2] T.S. Shih, C.H. Chang, Z.D. Ou, AFS Trans. **71**, 857-872 (1993).

[3] P. Prasad Rao, Susil K. Putatunda, Metall. Mater. Trans. **28A** (7), 1457-1470 (1997).

[4] E. Dorazil, Foundry M & T. **7**, 36-45 (1986).

[5] H. Krawiec, B. Stypuła, J. Stoch, M. Mikołajczyk, Corros. Sci. **48** (3), 595-607 (2006).

[6] H. Krawiec, Adv. Mater. Sci. **7** (2/12), 210-215 (2007).

[7] H. Krawiec, V. Vignal, J. Banaś, J. Electrochem. Soc. **153** (7), B231-B237 (2006).

[8] H. Krawiec, J. Lelito, E. Tyrała, J. Banaś, J. Solid State Electrochem. **13** (6), 935-942 (2009).

[9] A.L. Ortiz, F.L. Cumbrera, S. Sanchez-Bajo, F. Guiberteau, R. Caruso, J. Eur. Ceram. Soc. **20** (11), 1845-1851 (2000).